Draft version April 18, 2023
Typeset using LaTeX **twocolumn** style in AASTeX631

A Comprehensive Catalog of 52,631 Radial Velocity Standard Stars

Xiao-Xiao Ma [1,2] Jian-Jun Chen* [1,2] A-Li Luo* [1,2] Jing Chen [1,2] and Rui Wang [1]

[1] *CAS Key Laboratory of Optical Astronomy, National Astronomical Observatories, Chinese Academy of Sciences, Beijing 100101, China*
[2] *School of Astronomy and Space Science, University of Chinese Academy of Sciences, Beijing 100049, China*

ABSTRACT

We present a comprehensive catalog of 52,631 radial velocity standard stars (RV-STDs) in a unified system of radial velocity (RV) measurement by combining 5,505 stars refined from existing canonical catalogs and 47,126 stars extracted from the APOGEE DR17. These RV-STDs provide homogeneous sky coverage with the largest number of stars to date, and a typical observation time span of over 1000 days. The RV-STDs discovered in APOGEE exhibit a weighted standard deviation ($\sigma_{\rm RV}$) less than 200 $\rm m\,s^{-1}$ and contain more main-sequence and faint stars than previous works. Furthermore, we present three applications for this RV-STDs catalog: (i) A more moderate quadratic RV correction equation is provided for Gaia. (ii) A systematic offset of -6.13 $\rm km\,s^{-1}$ is verified in the Pilot Survey for LAMOST MRS. (iii) An RV zero point (RVZP) of 0.35 $\rm km\,s^{-1}$ is recommended to subtract for GALAH. All catalogs are be available at https://paperdata.china-vo.org/maxiaoxiao/four_catalogs.zip.

1. INTRODUCTION

Radial velocity (RV), which is a measure of the Doppler shift of a spectrum and reduced to the solar-system barycenter, is strictly defined as the *barycentric radial-velocity measure* (Lindegren & Dravins 2003). Although there are other types of radial velocity measures, such as *kinematic radial velocity* from geometry and *astrometric radial velocity* from astrometric observations, the distinction between them and the *barycentric radial-velocity measure* has been increasingly blurred in practice. Therefore, unless otherwise specified, any subsequent references to RV in this work pertain to the *barycentric radial-velocity measure* or *spectroscopic radial-velocity measure*. It is worth mentioning that all types of RV measures play significant roles in a wide range of studies or investigations on different scales.

In spite of this, the accuracy of RV varies greatly depending on the scale of the study. For example, a submeter per second level of accuracy is necessary for detecting and characterizing exoplanets (e.g., Udry & Santos 2007 and Rosenthal et al. 2021). On the other hand, a few $\rm m\,s^{-1}$ accuracy is sufficient for studying oscillations and pulsations in stars in order to gain insights into their internal structure and dynamics (e.g. Luhn et al. 2020 and Huber et al. 2019). However, for studies on a broader scale, such as spectroscopic binaries (e.g., Chen et al. 2022, which searched for extrinsic S-type stars in binary systems), the accuracy can be relaxed to several hundred $\rm m\,s^{-1}$ or even a few $\rm km\,s^{-1}$. This includes studies on Galactic structure and evolution (e.g. Xiang & Rix 2022, which investigated the Milky Way's early formation), as well as studies on the kinematics and mass distribution of the Galaxy (e.g., Newton et al. 2016, which presented the Galactic kinematics of mid M dwarfs in the solar neighborhood).

Over the past few decades, advancements in several areas have greatly improved RV measurements, thereby contributing substantially to the diverse studies mentioned above, particularly those requiring an accuracy of several hundred $\rm m\,s^{-1}$ or a few $\rm km\,s^{-1}$. Specifically, these advancements include: (i) The number and distribution of RV measurements has exponentially exploded owing to large-scale spectroscopic surveys, such as SDSS (Yanny et al. 2009), LAMOST (Deng et al. 2012; Luo et al. 2015; Liu et al. 2020), RAVE (Steinmetz et al. 2006), GALAH (De Silva et al. 2015) and Gaia-RVS (Katz et al. 2022). (ii) The computation of cross-correlation, which is a traditional but computationally intensive solution for RV, has been sped up thanks to hardware advances, such as GPU (Graphical Processing Units) parallel computing. For example, Zhao & Dumusque (2021) employed GPU to efficiently simulate stellar activity, including RVs. Additionally, distributed computing architectures like Hadoop have been used in astronomy, with Katz et al. (2022) calling the 2500 cores

Corresponding author: * Jian-Jun Chen; A-Li Luo
jjchen@nao.cas.cn lal@nao.cas.cn

of the Hadoop cluster to process the RV computation for the Gaia DR3. Spark, on the other hand, has been used in studies such as Wang et al. (2019), where a Spark cluster consisting of 15 PCs was employed to calculate the stellar parameters of about 3 million spectra for LAMOST MRS. (iii) The precision of RV measurements has improved significantly due to the development of algorithms. For instance, Brandt et al. (2020) developed a Python toolkit to automatically calibrate wavelength by a new algorithm of order-by-order extracting spectra. New techniques have also been adopted to boost the precision of RV measurements. For example, Li et al. (2008) enabled RV measurements with a precision of 1 $\mathrm{cm\,s^{-1}}$ using a laser frequency comb. (iv) The accuracy of RV measurements has been also advanced because of the search for radial velocity standard stars (RV-STDs), which are usually reviewed as benchmarks for RV corrections. Studies such as Udry et al. (1999a), Nidever et al. (2002), Chubak et al. (2012), Soubiran et al. (2013), Soubiran et al. (2018), and Huang et al. (2018) are dedicated to identifying those stars.

Despite the boom in observations, the growth of computational resources, and the improvement in precision, achieving the utmost accurate RV is still crucial as it is the cornerstone for all researches related to RV. A variety of factors can affect the accuracy of RV measurements, such as the absorption and scattering of light caused by the interstellar medium, as well as the design and resolution of the spectrometer and the processing pipeline for spectra. RV zero point (RVZP) is a powerful diagnostic tool for assessing the accuracy of RV measurements (Lindegren & Dravins 2003), as it takes into account diverse potential sources of error. For the accuracy of RV measurements from a spectroscopic survey, RVZP can be determined statistically by the residual between RV measurements and the "true" RVs of RV-STDs. Therefore, what is crucial for RVZP are a sufficient number of RV-STDs, wide sky coverage, and accurate RV values. However, existing catalogs may not be suitable for large spectroscopic surveys such as LAMOST and Gaia, which require extensive sky coverage and a massive amount of spectra. Furthermore, some so-called RV-STDs in those catalogs have not met the basic definition of an RV-STD, i,e., a star with multiple stable RV measurements over a long time span (e.g., Boulkaboul et al. 2022 found 27 stars in the catalog presented by Soubiran et al. 2018 failed to meet the RV-STD criteria used for calibrating Gaia-RVS). Moreover, some RV-STDs have been classified as the other object types like binaries, which are also no longer advisable to be used as RV-STDs.

To address the deficiencies and instability of current RV-STDs that have not been updated for a long time, we have built a general catalog of RV-STDs by reducing the existing catalogs of RV-STDs and searching for new RV-STDs from APOGEE. The remainder of the paper is organized as follows. The purification of existing canonical catalogs of RV-STDs will be presented in Section 2. The selection of RV-STDs from the APOGEE DR17 will be introduced in Section 3. Section 4 will detail the combination of these RV-STDs into a unified system and describe the data products, followed by the applications of RV-STDs in Section 5. Finally, the conclusions will be offered in Section 6.

2. EXISTING RV-STDS

2.1. *Canonical Catalogs of RV-STDs*

One of the most significant applications of RV-STDs is calibrating the RVZP of an object. To achieve this, numerous RV-STDs have been collected from many spectroscopic surveys or telescopes and their stability has gone through over a few decades. Benefiting from the advances in precision and accuracy of those RV-STDs, we selected databases including Udry et al. 1999a (hereafter U99a), Udry et al. 1999b (hereafter U99b), Nidever et al. 2002 (hereafter N02), Chubak et al. 2012 (hereafter C12) and Soubiran et al. 2018 (hereafter S18) as our benchmarks.

U99a is an official list of IAU RV standards, which was extended by U99b. Later on, N02 showed a difference of 0.053 $\mathrm{km\,s^{-1}}$ compared with U99a for the 26 stars in common. Using the RV measurements in N02, C12 established its own RVZPs in agreement within 0.01 $\mathrm{km\,s^{-1}}$. Moreover, S18 elaborated the differences or relations between S18 and the four other catalogs mentioned above. The successive consistency of these classic works and detailed discussions among them have made it possible to build a comprehensive catalog of RV-STDs in a unified RV measurement system. First, we provide a brief introduction to the five works.

Firstly, U99a released 38 FGK standard dwarfs that covers a considerable range in visual magnitudes from 4.27 to 7.64. As an IAU official set, the list was established thanks to the ELODIE (R = 42,000) and CORAVEL (R = 20,000) spectrometers, which ensured a precision level of 50 $\mathrm{m\,s^{-1}}$ and fulfilled the time baseline over 1000 days for ELODIE and 2500 days for CORAVEL.

Secondly, U99b extended the list proposed by U99a, which consisted of 107 stars whose RVs had been monitored with two CORAVEL spectrometers for more than 20 years. The velocity variation was kept within 0.3

$km\,s^{-1}$, and the RVs were given in the "ELODIE" system (U99a).

Thirdly, N02 provided a catalog of 889 late-type stars, of which 782 had a velocity scatter less than 100 $m\,s^{-1}$, making them potential RV-STDs. This catalog derived from observations taken between 1997 and 2001, during which the stars were typically observed 12 times with the HIRES echelle spectrometer on the 10-m Keck I telescope and with the "Hamilton" echelle spectrometer fed by either the 3-m Shane or the 0.6-m Coude Auxiliary Telescopes.

Fourthly, C12 gave precise RV measurements for 2046 nearby FGKM stars with an accuracy of 0.1 $km\,s^{-1}$ using the HIRES echelle spectrometer on the 10-m Keck I telescope. For 131 stars involved, a dozen years witnessed their stability with an RMS less than 30 $m\,s^{-1}$, resulting in viewing these 131 stars as RV-STDs.

Finally, S18 plays an important role in combination with all these catalogs. S18, a superseded version of Soubiran et al. 2013 (hereafter S13), compiled a dataset of 4813 stars with $\sim 71,000$ individual RV measurements collected by five spectrographs: ELODIE, SOPHIE, CORAVEL, HARPS and NARVAL. The homogeneity and precision of this dataset at a level of 300$m\,s^{-1}$ on a typical time baseline of 6 years satisfied the need for RV calibration of Gaia-RVS (Radial Velocity Spectrometer). The offsets between S18 and the four above catalogs, as elaborated in S18, provided a better understanding of how the RV measurements from various instruments can be merged into the same reference system.

2.2. *Selection*

Given that there may be some common sources among the five catalogs, we give priority to S18, followed by U99a and U99b, and finally C12 and N02 to avoid any duplicates. Additionally, we only select the stars that can be identified through SIMBAD to obtain supplementary information such as magnitudes in the U, B, V, J, H, K_s passbands for further analysis.

After selecting and removing the stars with invalid values, we further investigate the stability of these RV-STDs using the literature (Boulkaboul et al. 2022) and SIMBAD. The stars with one or more companions (i.e. binaries and/or multiplicities) that have been determined and those with volatile RV measurements re-observed by new surveys are filtered out (see Appendix A for more details). Table 1 presents an overview of the results of selecting the existing RV-STDs.

3. COMPLEMENTARY APOGEE RV-STDS

Table 1. Results of selecting RV-STDs

Catalog	N_{obs}	N_{sele}	N_{bin}	N_{com}
U99a	38	32	1	2
U99b	107	71	8	9
N02	782	579	5	59
C12	131	103	1	23
S18	4,814	4,737	76	153
APOGEE	657,135	47,126	252	[a] 16,345

NOTE— For each catalog, N_{obs} indicates the number of observed stars, while N_{sele} refers to the number of selected stars. N_{bin} presents the number of stars that are suspected to be binaries or multiplicities. N_{com} means the number of stars in common cross-matched with the APOGEE DR17.

[a] The number of common stars is obtained by cross-matching the 18,080 RV-STDs reported in H18 and the selected RV-STDs from the APOGEE DR17 in this work.

3.1. *APOGEE DR17*

Currently, the APOGEE project has completed two generations of surveys in the Milky Way, including APOGEE-1 (September 2011 to July 2014) and APOGEE-2 (August 2014 to January 2021). Using the 2.5-meter Sloan Foundation Telescope and the 1-meter NMSU Telescope at Apache Point Observatory (APO) in New Mexico, United States and the 2.5-meter Irénée du Pont Telescope of Las Campanas Observatory (LCO) in Atacama de Chile, APOGEE is able to acquire high-resolution spectra ($R \sim 22,500$) in the near-infrared (H-band;$1.51 - 1.70$ μm) with typical signal-to-noise ratios (SNR) greater than 100.

As the final data release used for this work, the APOGEE DR17 has collected a total of 657,000 unique targets and around 2,659,000 observations, providing a precision of ~ 0.2 $km\,s^{-1}$ for RVs and ~ 0.1 dex for 20 species of elemental abundances. Moreover, the rewritten programs for DR17 conclude a new RV analysis called Doppler (Nidever 2021), which enables more precise RV measurements than before, as well as an effort to improve RVs for faint stars.

3.2. *Filtering Rules*

Using the APOGEE DR14 data, which is only half of that available in the DR17, Huang et al. 2018 (hereafter H18) investigated RV measurements in APOGEE and released a new catalog containing 18,080 RV-STDs with a median stability of approximately 240 $m\,s^{-1}$. Follow-

ing in the footsteps of H18, we searched for more RV-STDs based on APOGEE DR17. As with S18, we apply strong RV-STD filtering rules to our work. However, it is important to highlight that the RV corrections for the existing RV-STDs in Section 2 differ between H18 and this work. This will be emphasized again in Section 4.1. Here are the rules we adopt to select RV-STDs from the APOGEE DR17:

For each RV-STD, there are

1. At least three individual visits with high-quality observed spectra (i.e., SNR ratio greater than 50 and radial velocity error less than 0.5 $\mathrm{km\,s^{-1}}$);
2. Over 200 days span from the filtered visits in Step 1;
3. $\overline{\mathrm{RV}}$ weighted standard deviation $\sigma_{\mathrm{RV}} \leq 0.2\ \mathrm{km\,s^{-1}}$,

where

- $\overline{\mathrm{RV}}$ is the weighted mean RV with a weight w_i applied to each RV measurement $\mathrm{RV_i}$ being $w_i = 1/\epsilon^2$ and ϵ the each radial velocity error;
- σ_{RV} is defined as

$$\sigma^2_{\mathrm{RV}} = \frac{\sum\limits_i w_i}{(\sum\limits_i w_i)^2 - \sum\limits_i w_i^2} \sum_i w_i(\mathrm{RV}_i - \overline{\mathrm{RV}})^2 \quad (1)$$

In Section 2.2, we exclude binaries or multiplicities in the reference catalogs. Similarly, in the RV-STDs from the APOGEE DR17, we exclude such cases. For each star,

1. the keyword `STARFLAG` 21$^{\mathrm{st}}$ (`MULTIPLE_SUSPECT`) binary digit which indicates that multiple components are apparent in the Gaussian decomposition of the cross-correlation is set to 0;
2. it is removed if the star with match with a star in the APOGEE Spectroscopic Binaries Value Added Catalog (see Kounkel et al. 2021);
3. it remains if the star is not identified as a binary in SIMBAD which is more discussed in Appendix A.

3.3. *Results*

The last column in Table 1 provides the results of selecting RV-STDs from the APOGEE DR17 and a total of 47,126 RV-STDs are identified. Figure 1 presents the summary statistics for the RV-STDs from the APOGEE DR17. What stands out in the figure is the time baseline and the number of observations are broadened, with values exceeding 3,000 days and 60 times, respectively. This strongly supports the stability of RV-STDs in conjunction with σ_{RV} less than 200 $\mathrm{m\,s^{-1}}$.

The sky distribution of the RV-STDs from APOGEE is shown on the celestial sphere in Figure 2. Over half of the RV-STDs are located in the northern sky, with more in the south compared to APOGEE DR14 due to the increasing collections by LCO. Our strong selection rules result in the elimination of 1,735 stars, while 30,781 new RV-STDs (in red) are added in DR17. These eliminations take place because of lower SNR or larger RV error compared to what the rule requires when additional observations are acquired. The remaining 16,345 RV-STDs are common in DR14 and DR17 and can be divided into two groups. Among these, a total of 13,876 RV-STDs (in grey) maintain their time baseline. The last 2,469 RV-STDs (in cyan) have a wider observing span than those in DR14, making them more credible RV-STDs than before.

In Figure 3, we provide a breakdown of the aforementioned 2,469 RV-STDs that were observed again during the session after the APOGEE DR14. The left panel shows that the additional observing days are distributed over a wide range of 3,000 days. In the right panel, we illustrate the distribution of the differences of mean weighted RV for the RV-STDs from the APOGEE DR17 and DR14. In the histogram, the red solid curved line shows the fit result using a Gaussian distribution with a mean of 0.3 $\mathrm{km\,s^{-1}}$ and a standard deviation of 0.21 $\mathrm{km\,s^{-1}}$. This result aligns well with the statistical summary in H18. The RV-STDs with a larger time baseline and consistently stable RV measurements throughout the survey are more reliable than the others from APOGEE.

Figure 4 demonstrates the distribution of atmospheric parameters (i.e., logg, $\mathrm{T_{eff}}$, [Fe/H]) for the RV-STD samples. It is noteworthy that the number of dwarfs is comparable to that of giants, despite the majority of APOGEE targets being red giants (Zasowski et al. 2017). In addition, over 90% of the objects are FGK-type stars, and approximately 20% are metal-poor ([Fe/H] < -0.4 dex) stars. The broader range of stellar types facilitates more extensive investigations into the velocity scales and RVZPs of different surveys.

4. A COMPREHENSIVE CATALOG OF RV-STDS

4.1. *To a Unified RV Measurement System*

Because of a variety of physical effects such as gravitational redshifts and effects within stellar atmospheres (Lindegren & Dravins 2003), as well as limitations of

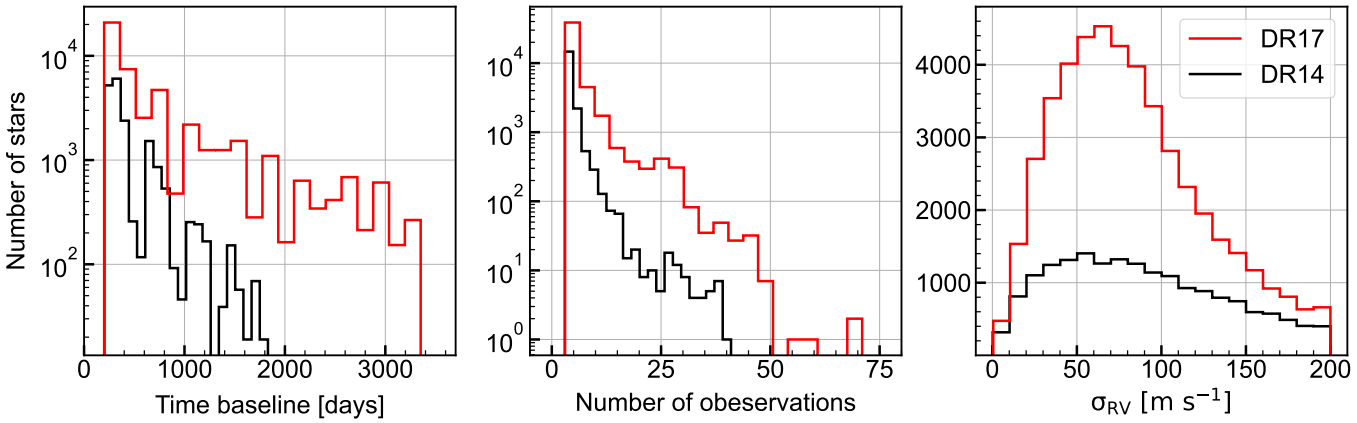

Figure 1. Histograms of time baselines, number of observations and σ_{RV} from left to right. The RV-STDs from the APOGEE DR17 (this work) and DR14 (H18) are shown in red and black, respectively.

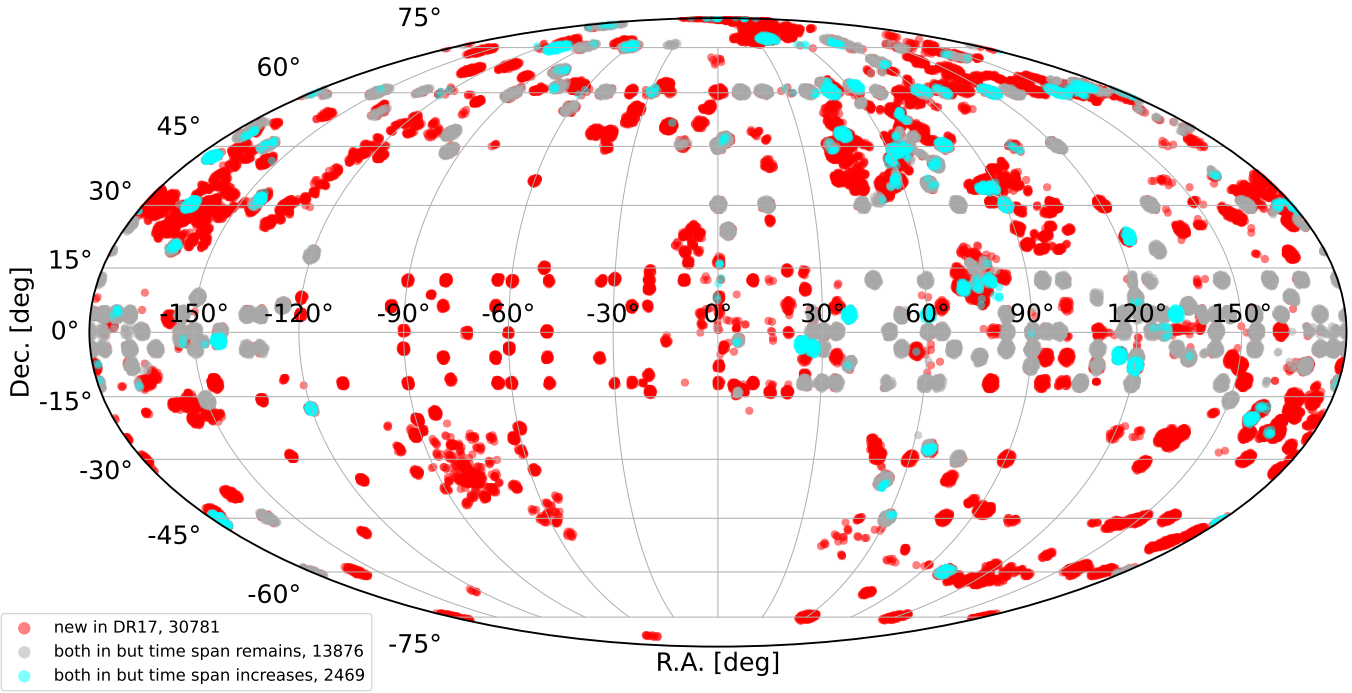

Figure 2. Distribution of the RV-STDs from APOGEE using a Mollweide projection in galactic coordinate frame. The three color codes indicate three individual groups. The red dots are the RV-STDs rediscovered in DR17 but not in DR14. The remaining dots are the common RV-STDs which can be categorized into two groups. The grey dots represent the RV-STDs with a maintained time baseline, while the cyan dots represent those with an extended observing time.

instruments such as the resolution and design of a spectrometer (Tsantaki et al. 2022), there is an avoidable RVZP between an RV measurement and the "true" RV during the observation of an object. Although obtaining the "true" RV may not be feasible, an RV measurement in a unified reference system is acceptable. We choose SOPHIE as our target reference system as it offers complete descriptions of the distinctions between each instrument and SOPHIE itself, as outlined in S18. Each spectroscopic instrument corresponds to a single RV measurement system. We divide the unification process into two parts, respectively for the RV-STDs from existing catalogs and those from the APOGEE data.

The RV measurements in the instrumental frames of U99a, U99b, N02, and C12 are initially converted to align with the SOPHIE frame, as described in S18. Table 2 provides a summary of the transformations to align with SOPHIE. As a result, the conversions in S18 is used instead of S13. We note that the respective transformations between the two references are slightly different.

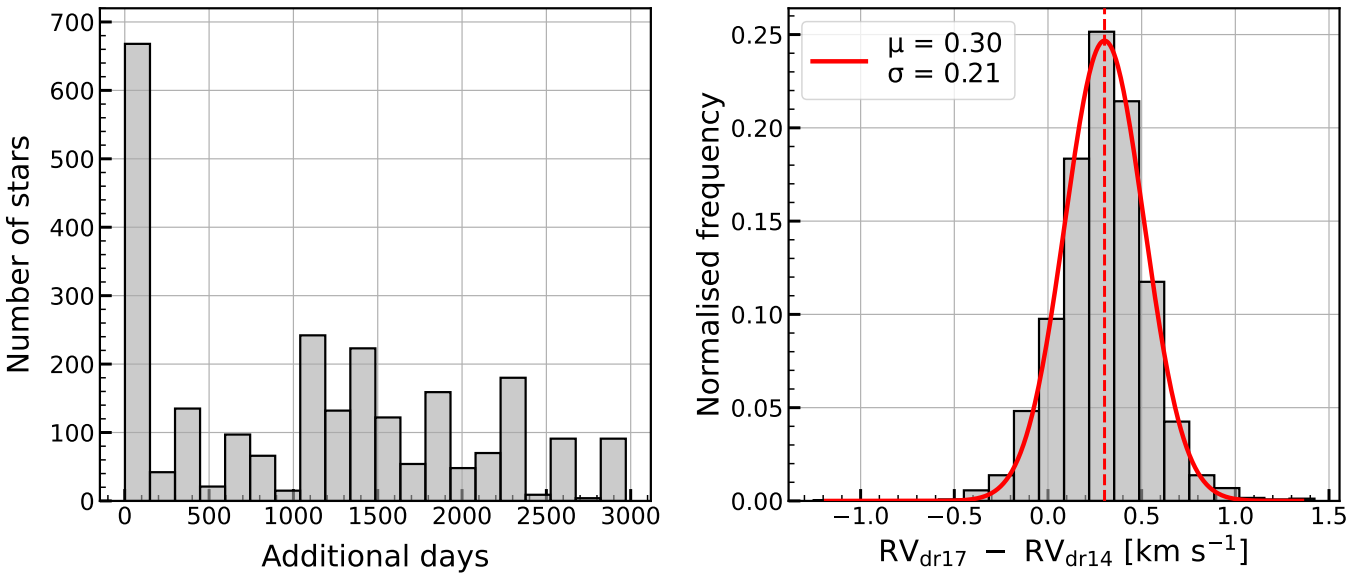

Figure 3. Histograms of additional days and differences of RV for 2479 reassured RV-STDs. The *left panel* presents the distribution of additional observing days compared to the APOGEE DR14. The *right panel* illustrates the normalised distribution of the differences of mean weighted RV for these RV-STDs. The solid curved line shows the result of fitting the histogram using Gaussian distribution.

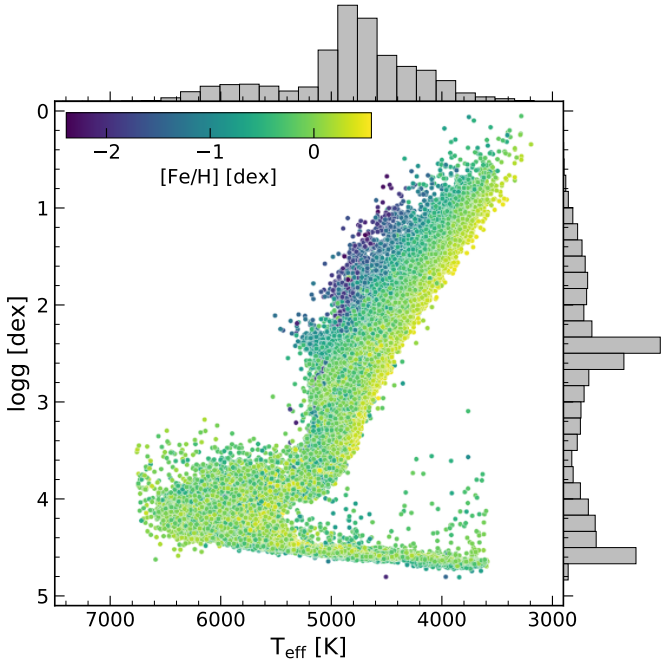

Figure 4. Kiel diagram of the RV-STDs from the APOGEE DR17. Histograms of effective temperature (T_{eff}) and surface gravity (logg) are also shown in the *top* and *right panel*, respectively. The color bar denotes metallicity ([Fe/H]).

Next, the APOGEE DR17 is cross-matched with the combination of the five transformed catalogs and 256 stars in common are identified. After eliminating abnormal or null data via iterative 3-sigma clipping and data cleaning, a total of 225 stars remain. Using these 225 stars, we fit the RV differences between APOGEE and the combination of the five catalogs as a function of T_{eff} to calibrate the RV measurements of the APOGEE RV-STDs in the same reference frame as SOPHIE. The results are set out in Figure 5, and the trend (in red) is consistent with H18 (in blue). As T_{eff} increases, a larger offset emerges and reaches 0.2 km s^{-1} for F-type

Table 2. Transformations of the existing RV-STDs

Catalog	S13	S18
U99	259.0(B − V) − 105.2	63.2(J − K) − 16.7
N02	72 [a]	26
	-141 [b]	
C12	63 [a]	72
	-98 [b]	

NOTE— The calibration formulae are relative to the RV difference between SOPHIE and the other instruments and are expressed in m s^{-1}. Given that the RV measurements of both U99a and U99b are provided in the ELODIE system, they share the same transformation.

[a] The template of the Sun

[b] The template of an M dwarf

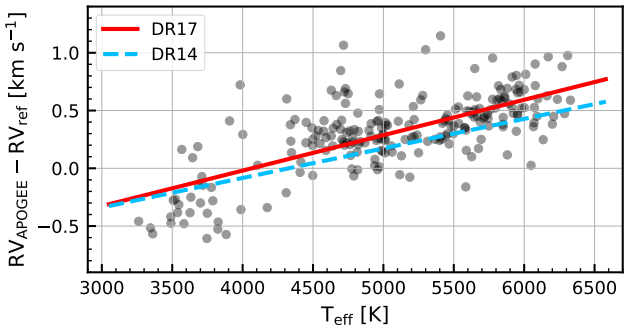

Figure 5. Differences in the RV measurements between APOGEE and the five reference catalogs for common stars as a function of T_{eff}. The red solid line fits the linear trend with T_{eff}, and the blue dashed line provides the same fitting result obtained by H18.

star. The fitting Equation (2) is applied to calibrate the RVZPs from the APOGEE DR17 to the reference frame.

$$\Delta RV = 0.3065 \times (T_{eff}/10^3\ K) - 1.2459\ km\,s^{-1} \quad (2)$$

To decouple the gravity or/and metallicity trends, we also fit the trend with them. For logg, the common RV-STDs are binned in increments of 0.5 dex, and for [Fe/H], they are binned in a step of 0.25 dex. It can be seen in Figure 6 that there is no significant trend in the RV differences with logg (represented by the blue solid line) or [Fe/H] (represented by the green solid line). However, What is striking in the figure is a similar RV offset of 0.35 km s^{-1} for both of them (in the red dashed lines), as also reported in the APOGEE DR12 by Nidever et al. (2015). We have not corrected the RVs for any offsets in the current analysis.

4.2. *Data Products*

After combining the RV-STDs from five reference catalogs in Section 2 and extracting those from the APOGEE DR17 in Section 3, we compile a comprehensive catalog of 52,631 RV-STDs. The RV measurements are placed in the same system, SOPHIE, in Section 4.1. For 17 common stars, the RV measurements and relevant information are sourced from APOGEE instead of the reference catalogs.

Presented below is an inventory of the data products that are produced as a result of this study.

1. A comprehensive catalog of 52,631 RV-STDs in combination of the reference and the APOGEE DR17 (Table 3);

2. A catalog containing 5,522 RV-STDs chosen from the canonical catalogs (Table 4);

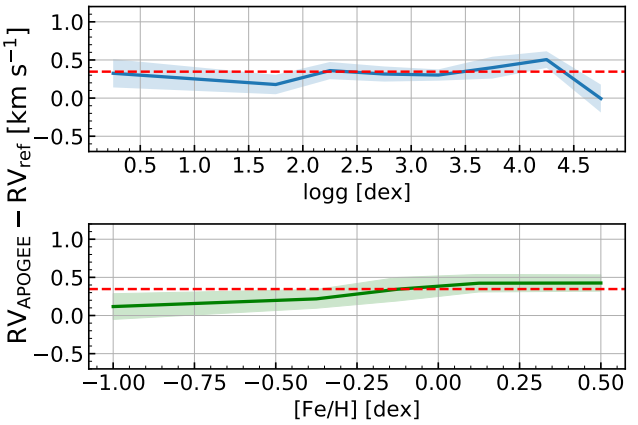

Figure 6. As Figure 5, but as a function of logg in the *top panel* and [Fe/H] in the *bottom panel*. The means and standard deviations for the RV-STDs in each bin of atmospheric parameters are shown as solid lines and shaded areas, respectively. The red dashed lines indicate the mean RV differences of the overall RV-STDs.

3. A catalog presenting 47,126 RV-STDs extracted from the APOGEE DR17 (Table 5);

4. A catalog of 249,012 reliable RV measurements corresponding to the 47,126 RV-STDs sourced from the APOGEE DR17 (Table 6).

All catalogs can be accessible online.[1]

As seen in Figure 7, the RV-STDs are uniformly and homogeneously distributed throughout the entire sky after combination. Figure 8 provides a statistical summary of these RV-STDs, which cover a wide time span and multiple observations, with the majority having RVs less than 400 km s^{-1}. Figure 9 further presents their distribution in terms of their brightness (H magnitude) and temperature (J − K color index). Since most of the samples in the final catalog are from APOGEE, the RV-STDs primarily pertain to red giants, as detailed by Zasowski et al. (2017). Specifically, 75% of the RV-STDs exhibit J − K values greater than 0.5, with a broad scope of luminosity relative to the H magnitude, varying from -1 to 14 mag.

[1] https://paperdata.china-vo.org/maxiaoxiao/four_catalogs.zip

Table 3. Comprehensive Catalog of 52,631 RV-STDs in Combination of the Reference and the APOGEE DR17

Index	Label	Format	Units	Description
1	ID	String	···	HD/HIP/TYC/2MASS/APOGEE identification
2	from	String	···	U99a/U99b/N02/C12/S18/APOGEE
3	RA	Float	deg	R.A. (J2000)
4	DEC	Float	deg	Decl. (J2000)
5	is_calib	Bool	···	Flag that indicates whether RV of a star is calibrated [a]
6	RV	Float	$\mathrm{km\,s^{-1}}$	Calibrated RV measurement [b]
7	sigma_RV	Float	$\mathrm{km\,s^{-1}}$	Uncertainty or error of RV measurement from a specified catalog [c]
8	Delta_T	Integer	days	Time span
9	N	Integer	···	Number of visits [d]
10	J	Float	mag	Apparent magnitude from J passband
11	H	Float	mag	Apparent magnitude from H passband
12	K	Float	mag	Apparent magnitude from K_s passband
13	J-K	Float	mag	J minus K_s

NOTE— This table is available in its entirety online in machine-readable form. A portion is shown here for guidance regarding its form and content.

[a] Due to the absence of the necessary factor, J − K or $T_{\rm eff}$, the RV measurements of certain reference RV-STDs cannot be transferred to the SOPHIE system for calibration.

[b] For the reference RV-STDs, the equations listed in column 'S18' of Table 2 are calculated. For the APOGEE RV-STDs, Equation 2 is employed. As for those that have not been calibrated, the RV values obtained from the raw catalog are used.

[c] The values of $\sigma_{\rm RV}$ are copied from the original catalogs for each RV measurement. However, $\sigma_{\rm RV}$ values are not available for U99a and N02. For the APOGEE DR17, $\sigma_{\rm RV}$ values are computed using Equation 1.

[d] N02 does not provide any data on N.

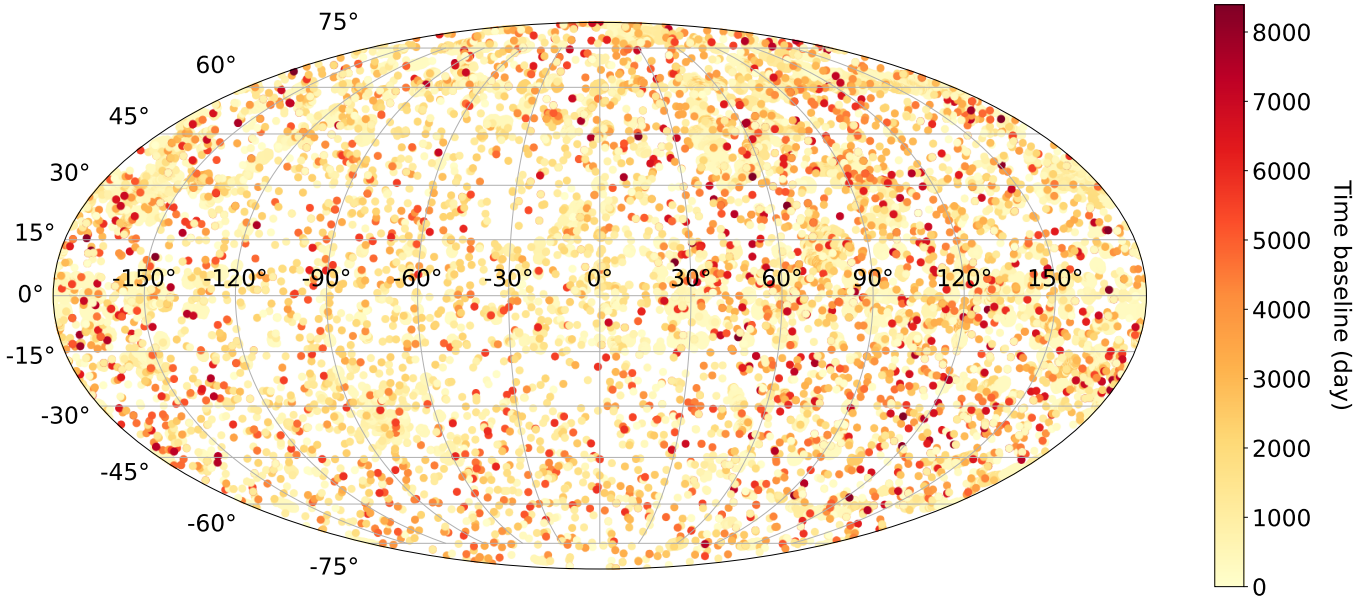

Figure 7. Distribution of all the RV-STDs in combination of the reference catalogs and the APOGEE DR17 using a Mollweide projection in galactic coordinate frame. The color denotes the time span of each RV-STD.

Table 4. The 5,522 RV-STDs Chosen from the Canonical Catalogs

Index	Label	Format	Units	Description
1	ID	String	···	HD/HIP/TYC/2MASS identification
2	from	String	···	U99a/U99b/N02/C12/S18
3	RA	Float	deg	R.A. (J2000)
4	DEC	Float	deg	Decl. (J2000)
5	RV_S18	Float	$\mathrm{km\,s^{-1}}$	Calibrated RV measurement using the equations listed in column 'S18' of Table 2
6	RV_S13	Float	$\mathrm{km\,s^{-1}}$	Calibrated RV measurement using the equations listed in column 'S13' of Table 2
7	RV_raw	Float	$\mathrm{km\,s^{-1}}$	Raw RV measurement obtained from the reference catalogs
9	sigma_RV	Float	$\mathrm{km\,s^{-1}}$	Uncertainty or error of RV measurement from a specified catalog
10	Delta_T	Integer	days	Time span
11	N	Integer	···	Number of visits
12	B	Float	mag	Apparent magnitude from B passband
13	V	Float	mag	Apparent magnitude from V passband
14	B-V	Float	mag	B minus V
15	J	Float	mag	Apparent magnitude from J passband
16	H	Float	mag	Apparent magnitude from H passband
17	K	Float	mag	Apparent magnitude from K_s passband
18	J-K	Float	mag	J minus K_s

NOTE— This table is available in its entirety online in machine-readable form. A portion is shown here for guidance regarding its form and content.

Table 5. The 47,126 RV-STDs Extracted from the APOGEE DR17

Index	Label	Format	Units	Description
1	ID	String	···	APOGEE identification copied from `apogee_id`
2	RA	Float	deg	R.A. (J2000)
3	DEC	Float	deg	Decl. (J2000)
4	RV	Float	$\mathrm{km\,s^{-1}}$	Weighted mean RV measurement
5	RV_calib	Float	$\mathrm{km\,s^{-1}}$	Calibrated RV
6	sigma_RV	Float	$\mathrm{km\,s^{-1}}$	RV standard deviation computed by Equation 1
7	Delta_T	Integer	days	Time span
8	N	Integer	···	Number of visits that meet the selection criteria for computation
9	SNR	Float	···	Average signal to noise ratio
10	TEFF	Integer	K	Effective temperature
11	J	Float	mag	Apparent magnitude from J passband
12	H	Float	mag	Apparent magnitude from H passband
13	K	Float	mag	Apparent magnitude from K_s passband
14	J-K	Float	mag	J minus K_s

NOTE— This table is available in its entirety online in machine-readable form. A portion is shown here for guidance regarding its form and content.

Table 6. The 249,012 Visits Corresponding to the RV-STDs from APOGEE

Index	Label	Format	Units	Description
1	APOGEE_ID	String	···	APOGEE identification copied from `apogee_id`
2	VISIT_ID	String	···	APOGEE visit identification copied from `visit_id`
3	RV	Float	$\mathrm{km\,s^{-1}}$	Heliocentric RV measurement
4	RV_err	Float	$\mathrm{km\,s^{-1}}$	RV error
5	MJD	Integer	day	Modified Julian Date of this visit
6	SNR	Integer	···	Average signal to noise ratio

NOTE— This table is available in its entirety online in machine-readable form. A portion is shown here for guidance regarding its form and content.

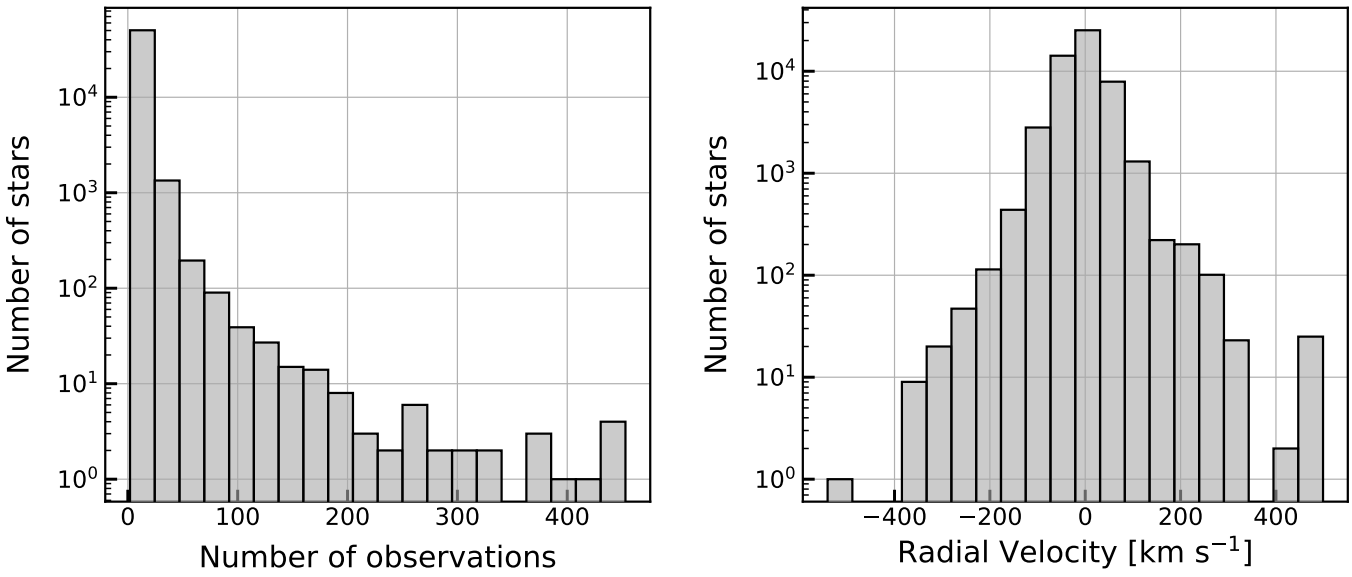

Figure 8. Histograms of number of observations and RVs for all 52,631 RV-STDs after combination.

5. APPLICATIONS

In this section, we calibrate the RVZPs of Gaia DR3, LAMOST MRS DR9, RAVE DR3 and GALAH DR3 based on their unique characteristics and analyze their potential tendencies of atmospheric parameters. Consequently, we evaluate the residuals by computing the differences between the RV measurements of each survey and the corresponding RV-STDs. Appendix B details how to filter out the common stars that do not meet the required quality standards prior to comparison.

In order to generally define the "relative" differences between one ground-based catalog and the catalog of this work, we use a pair of statistical terms that serve as the boundaries of the 68.3% confidence interval. These terms are adopted from the accuracy assessment of RVs in the Gaia DR3 catalog (Katz et al. 2022). They are defined as:

$$\epsilon_{\mathrm{acc}}^{\mathrm{low}} = \sqrt{\frac{\pi}{2N}} \left(\tilde{V}_{\mathrm{R}}^{\mathrm{res}} - Per\left(V_{\mathrm{R}}^{\mathrm{res}}, 15.85\right) \right) \tag{3}$$

$$\epsilon_{\mathrm{acc}}^{\mathrm{upp}} = \sqrt{\frac{\pi}{2N}} \left(Per\left(V_{\mathrm{R}}^{\mathrm{res}}, 84.15\right) - \tilde{V}_{\mathrm{R}}^{\mathrm{res}} \right), \tag{4}$$

where $N, \tilde{V}_{\mathrm{R}}^{\mathrm{res}}, Per\left(V_{\mathrm{R}}^{\mathrm{res}} 15.85\right), Per\left(V_{\mathrm{R}}^{\mathrm{res}}, 84.15\right)$ are the number of stars, the median, the 15.85^{th} and 84.15^{th} percentiles of the distribution of RV residuals in each bin, respectively.

5.1. *Calibration of Known Issues*

It is commonplace that various issues that could influence RV measurements emerge in in-depth studies on surveys and/or the growing utilization of telescopes. Depending on the defects of the instruments, the precision of the methods applied to calculate RV, or even the environments of the observation, the accuracy of RV mea-

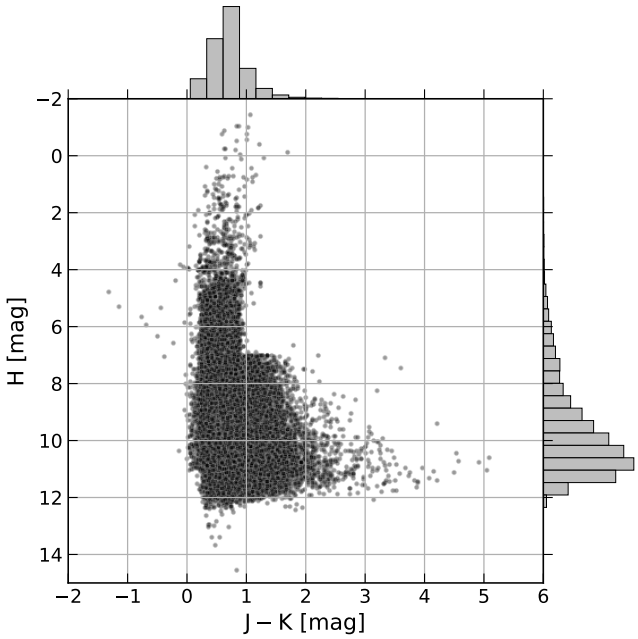

Figure 9. H v.s. J − K Color-Magnitude Diagram (CMD) of the 52,631 final combined RV-STDs. Histograms of J-K color index and H magnitude are also given in the top and right panel, respectively.

surements can be more or less affected. Regardless of the issue, it is critical to locate the factor that contributes the most to the accuracy of the RV measurements and correct it.

(i) *Gaia DR3.* In Katz et al. (2022), RVs from Gaia DR3 were reported to show a quadratic G_{RVS} magnitude trend, which could be due to traps in the CCD pixels. As illustrated in Figure 10, this trend (in red solid curve) persist and is modelled by Equation (5). However, the new model (in black dot-dash line) reveals a slight systematic offset of 20 $m\,s^{-1}$ for the stars brighter than $G_{RVS} = 11$ mag when compared with the model (in blue dashed line) fitted by Katz et al. (2022). This offset falls within the limit of the RV measurement of the Gaia Radial Velocity Spectrometer (RVS) and can be neglected. For the stars fainter than $G_{RVS} = 11$ mag, the increasing residual trend with G_{RVS} is mitigated and declines from 0.4 $km\,s^{-1}$ to 0.2 $km\,s^{-1}$ at $G_{RVS} = 14$ mag. This is because the residuals provided by Gaia DR3 are conservative, taking into account a significant proportion of stars that may have variable RVs, such as binaries. Moreover, the measurements of stellar parameters for fainter stars are poorer because of low SNR, but the stars used in the comparison have high quality after filtering (see Appendix B for more details).

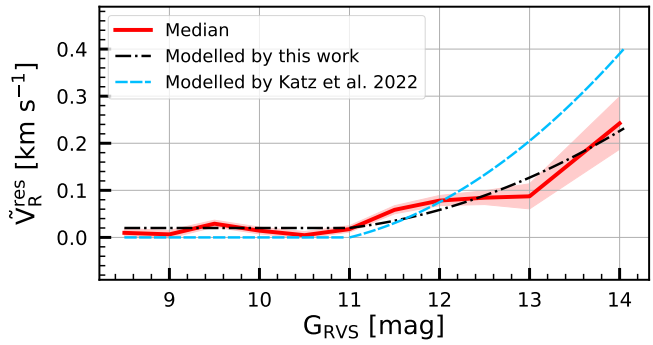

Figure 10. Median residuals of the RV as a function of G_{RVS} magnitude (red solid curve) with the fitted correction model over-plotted (black dot-dash line for this work and blue dashed line from the literature). The red shaded areas indicate the 68.3% confidence interval on the medians of the residuals of RVs.

$$\Delta RV\ km\,s^{-1} = \begin{cases} 0.020 & \text{if } G_{RVS} < 11 \\ 1.597 - 0.310 \times G_{RVS} + 0.015 \times G_{RVS}^2 & \text{else.} \end{cases} \quad (5)$$

(ii) *LAMOST MRS DR9.* According to Zhang et al. (2021) and Wang et al. (2019), a significant systematic offset of around -6 $km\,s^{-1}$ was verified for the stars observed during the LAMOST Pilot Survey. Such a large deviation was caused by the use of the scandium (Sc) lamp instead of the later thorium-argon (ThAr) lamp for wavelength calibration. In order to investigate this deviation with a larger sample size, we use observations as our subject instead of stars (see Appendix B for more details). We divide the samples into two groups: one consists of the observations from the Pilot Survey (from September 2017 to May 2018), during which most of the spectra were calibrated using the Sc lamp, and the other includes the observations from the Formal Survey (from August 2018 to June 2021), in which the ThAr lamps were fully utilized. What stands out in Figure 11 is a deviation of -6.13 $km\,s^{-1}$ compared to the RV-STDs, which confirms the wavelength calibration issue mentioned above. Another small peak near -1 $km\,s^{-1}$ is also observed, possibly due to a fraction of observations with wavelength calibrated by the ThAr lamp during the Pilot Survey. As a historical legacy, the calibration lamp issue should be noted by users of LAMOST. To address this issue, LAMOST recommends using the cal-

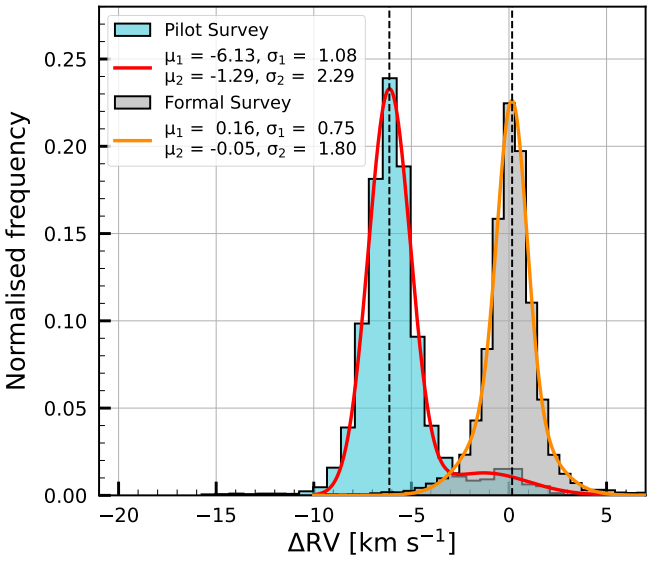

Figure 11. Histograms of the RV differences for 6,916 observations of the Pilot Survey and 18,337 observations of the Formal Survey compared with the RV-STDs. Both of these are fitted with two Gaussians, represented as the red and orange solid curves.

ibrated RVs with the suffix `1` [2], such as `rv_b1`, `rv_r1`, `rv_br1` and `rv_lasp1`.

5.2. *RVZPs*

Essentially, the RVZP represents the deviation of a particular spectrum's wavelength solution from its actual wavelength solution in terms of RV. This deviation can be evaluated by computing the difference between the RV measurement of a given spectrum and the true RV value of the star corresponding to that spectrum. As mentioned in Section 4.1, it is impossible to have access to the "true" RV value of a star. As a consequence, statistical residuals of RV-STDs between their RV measurements and RVs based on multiple visits within a long time span can be used as an alternative to the "true" RVZPs. Figure 12 illustrates such statistical residuals to show the systematic RVZPs for Gaia, LAMOST, RAVE and GALAH, respectively.

After applying calibration using Equation (5), Gaia (as shown in the top left panel of Figure 12) displays no significant RVZPs and a scatter of $\sigma < 1$ km s^{-1}. This level of scatter is comparable to the RV precision of Gaia-RVS for relatively bright stars (Cropper et al. 2018). For the overall RV measurements of LAMOST MRS (as shown in the top right panel of Figure 12), after calibrating the RV measurements during the Pilot Survey, there is an offset of 0.15 km s^{-1} with a scatter of 0.9 km s^{-1}, which meets the scientific goals and survey plans of LAMOST MRS proposed by Liu et al. (2020) in terms of RV uncertainty.

Regarding RAVE (shown in the bottom left panel of Figure 12), the RVZP has decreased to -0.1 km s^{-1} compared to a systematic offset of -0.32 km s^{-1} reported by Steinmetz et al. (2020). The latter study used the Gaia DR2 catalog as the benchmark, which was shown to have its own systematic bias (Sartoretti et al. 2018). As expected, this decrease in RVZP is because the significant RVZPs greater than 0.2 km s^{-1} have been overcome based on the RV-STDs found in this work. The large standard deviation of 1.36 km s^{-1}, which is similar to the value of 1.2 km s^{-1} mentioned in Steinmetz et al. (2020), can be explained by the reasons given in the literature.

For GALAH, the standard deviation of its RVZPs is 0.33 km s^{-1}, consistent with the value reported by Buder et al. (2021). However, the recorded offset of -0.02 km s^{-1} may be underestimated compared to the RVZP of 0.35 km s^{-1} shown in the bottom right panel of Figure 12. This underestimation is due to the comparison catalog used by GALAH DR3, which set APOGEE DR16 as its benchmark. Both Zasowski et al. (2017) and Section 4.1 have shown that APOGEE has an offset of 0.35 km s^{-1}. Therefore, it is highly recommended to subtract a systematic deviation of 0.35 km s^{-1} when using the RV `rv_nogr_obst` of GALAH DR3.

5.3. *Atmospheric parameter trends*

Strictly speaking, all the RVs mentioned above, which are derived from spectra, are not a physical velocity but a *barycentric radial-velocity measure* (Lindegren & Dravins 2003). Almost all traditional methods for solving RVs from spectra utilize the template matching method, and there is no exception for the pipelines of Gaia, LAMOST, RAVE, and GALAH. The atmospheric parameters are the most basic components of the spectra templates, and the distribution and step of the parameter space directly determine the goodness of match with the spectra, which in turn affects the solution of the RV measurements. It is therefore important to explore the RV residuals as a function of atmospheric parameters, which can help identify the general issues and improve the data processing of spectra. Figure 13 illustrates such trends of the RV residuals as a function of binned parameters.

Concerning logg and [Fe/H], there are no significant trends for Gaia, LAMOST and RAVE. However, what

[2] The documentation of the LAMOST MRS General Catalog provides more detailed descriptions on RV, which can be found at the following link: http://www.lamost.org/dr8/v2.0/doc/mr-data-production-description#s3.1

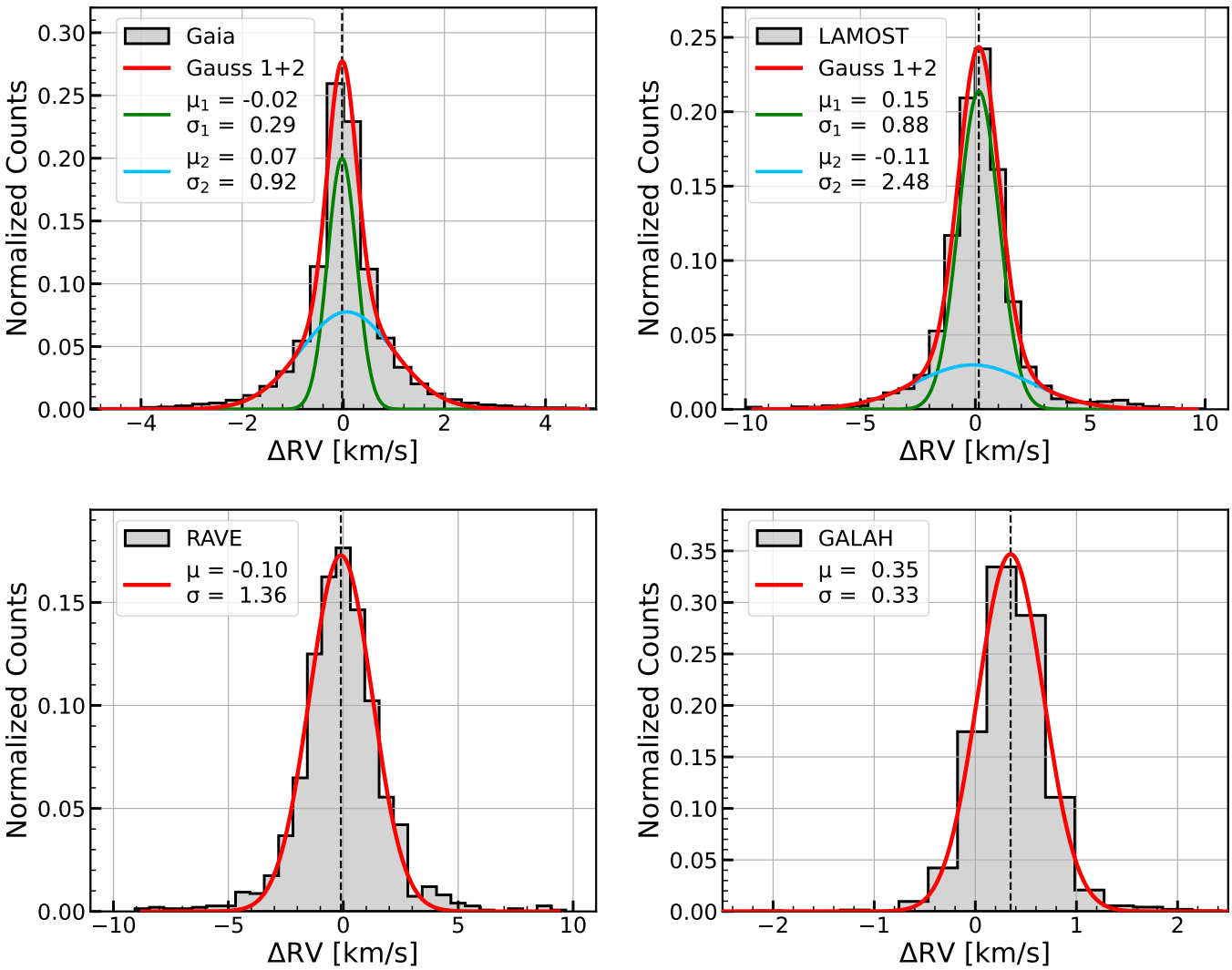

Figure 12. Distribution of the residuals of the common stars between the RV measurements from the ground-based catalogs and the RVs from the RV-STDs. After addressing the known issues described in Section 5.1, the residuals of Gaia DR3 (*top left*) and LAMOST MRS DR9 (*top right*) are fitted with red solid curves using two Gaussians, with narrow and wide components represented by green and blue solid lines, respectively. Meanwhile, the residuals of RAVE DR6 (*bottom left*) and GALAH DR3 (*bottom right*) are fitted with red solid curves using a single Gaussian.

is striking in Figure 13 is GALAH demonstrates a positive correlation trend for both logg and [Fe/H], with an increase of up to 0.5 $\mathrm{km\,s^{-1}}$ in the range of the corresponding parameters.

In terms of $T_{\rm eff}$, all four catalogs show the residuals of RV measurements increase with $T_{\rm eff}$. This can be attributed to spectra templates being more sensitive to $T_{\rm eff}$ than the other two parameters, logg and [Fe/H]. In other words, the spectral classification plays a dominant role in determining the accuracy of RV measurements, as evidenced by the existence of two RVZPs in N02 and C12 (as shown in Table 2), depending on the template of the spectral classification. Therefore, it is essential to consider the impact of the use of a set of templates, particularly the atmospheric parameters, on the accuracy and precision of RV measurements.

6. CONCLUSIONS

We compile a comprehensive catalog of 52,631 RV-STDs using data from the APOGEE DR17 and existing datasets of RV-STDs. For the RV-STDs drawn from the APOGEE DR17, the visits with at least three times and a time span of over 200 days ensure the stability of these RV-STDs with $\sigma_{\rm RV}$ less than 200 $\mathrm{m\,s^{-1}}$. In order to purify the samples, we meticulously curate the RV-STDs from the existing datasets and remove the objects that fail to meet the definition of RV-STD, e.g., spectroscopic binaries, as identified by the state-of-the-art literature and SIMBAD. We calibrate all RV-STDs to

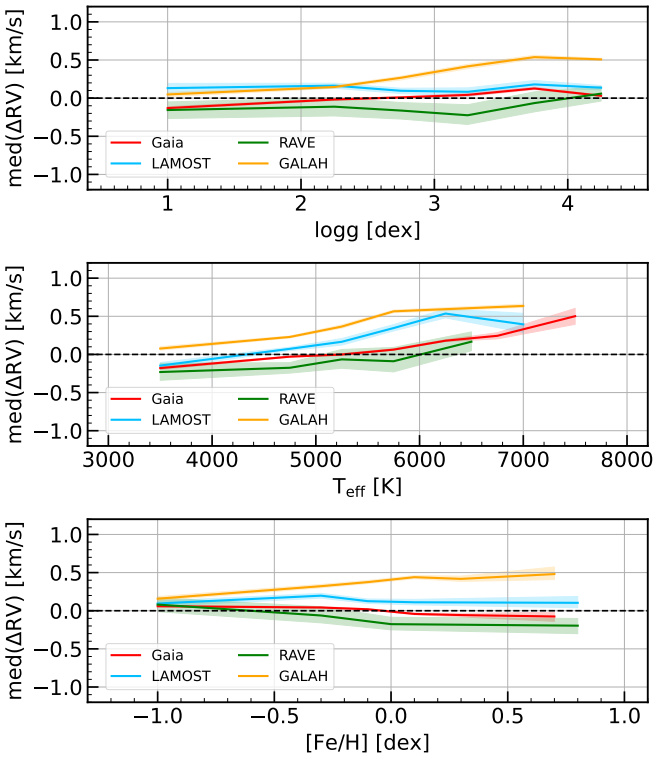

Figure 13. Median residuals of the RV against atmospheric parameters, i.e., surface gravity (logg), effective temperature (T_{eff}) and metallicity ([Fe/H]), arranged from top to bottom. The four surveys are represented by four different colors. The red shaded areas denote the 68.3% confidence interval on the median RV residuals.

a common system using SOPHIE as a uniform baseline. The development of APOGEE-2 and the combination of RV-STDs from the past two decades have enabled us to establish a dense and uniform RV-STD sample, particularly in the southern sky. The uniformity and density of this sample, as well as its coverage across the sky, provide more calibration target options for observations and offer valuable information in the Kiel Diagram for a wide range of stellar types. Nonetheless, The lack of high-velocity (the absolute value of RV $\geq$ 500 $\mathrm{km\,s^{-1}}$) RV-STDs prevents in-depth studies on stellar dynamics concerning the impact of gravitational forces. This vacancy is expected to be filled in the future since Katz et al. (2022) claimed that epoch RVs will be published in Gaia DR4, which will provide a larger RV-STD sample. Furthermore, while the comprehensive catalog includes RVs in a unified reference system, the error or uncertainty of RV measurement varies across sources. We therefore indicate the origin of each RV-STD in the table with the keyword `from` and provide users with two sub-catalogs derived from APOGEE and a canonical reference dataset to allow for flexible use according to specific tasks.

As applications, we use the catalog to investigate the RV measurements of the Gaia DR3, LAMOST MRS DR9, RAVE DR6 and GALAH DR3. Initially, the known issues of Gaia and LAMOST MRS are corrected by applying an offset as a function of G_{RVS} and a systematic bias of -6.13 $\mathrm{km\,s^{-1}}$ identified in the Pilot Survey. After correction, the RV measurements of Gaia and LAMOST MRS show similar statistical properties to those described in their respective references. While the RVZP of RAVE DR6 is reduced to -0.1 $\mathrm{km\,s^{-1}}$, that of the GALAH DR3 is raised to 0.35 $\mathrm{km\,s^{-1}}$, which is worth drawing the attention of users. In terms of atmospheric parameter trends, the RV residuals of all four surveys indicate a positive trend in effective temperature. However, for more detailed exploration of RV, it is crucial to consider the pipelines of data processing, the design characteristics of instruments, and the observational circumstances. Although the comprehensive catalog offers valuable insights, further investigation demands a more thorough analysis to provide touchstones of comparisons for both RVZPs and the velocity scales of the various instruments and observatories.

7. ACKNOWLEDGEMENTS

This work is supported by Supported by National Key R&D Program of China (grant No. 2019YFA0405102), and National Science Foundation of China (grant No. U1931209, 12103068, 11973060 and 12090044). Guoshoujing Telescope (the Large Sky Area Multi-Object Fiber Spectroscopic Telescope, LAMOST) is a National Major Scientific Project built by the Chinese Academy of Sciences. Funding for the Project has been provided by the National Development and Reform Commission. LAMOST is operated and managed by the National Astronomical Observatories, Chinese Academy of Sciences.

APPENDIX

A. CONTAMINATION

In Section 2.2 and Section 3.2, the RV-STD samples from the existing canon and the APOGEE DR17 are both purified using SIMBAD. By utilizing the `main_type` keyword within SIMBAD, it is possible to determine the classification of a given object. The samples consisting of `**`, `SB*`, `EB*` in `main_type`, which specifically refer to 'double or multiple stars', 'eclipsed binaries', and 'spectroscopic binaries', respectively, are not

present as RV-STDs. In addition, some of the targets categorized as `galaxy` are also excluded.

B. COMPARISON SAMPLE

In Section 5, the RV measurements of the Gaia DR3, the LAMOST MRS DR9, the RAVE DR6 and the GALAH DR3 are evaluated by the residuals of RV between them and the RV-STDs collected in this work. The selection and filtering of the common samples are described below.

Gaia DR3. The data we use is the main source catalog of the Gaia DR3, `gaiadr3.gaia_source`, which is from the Gaia ESA Archive: https://gea.esac.esa.int/archive/ . The stars that fail to meet the following quality criteria are removed: (i) `rv_expected_sig_to_noise` $\geq$ 5, (ii) valid `grvs_mag` and `radial_velocity` and (iii) valid atmospheric parameters, i.e., `logg_gspphot`, `teff_gspphot` and `mh_gspphot`. In order to cover more stars to analyse the known issues in Section 5.1 and the RVZPs in Section 5.2, the last point is not necessary except for the assessment of atmospheric parameter trends in Section 5.3. For the Gaia DR3, the former larger comparison dataset contains 45,717 stars and the other 30,710.

LAMOST MRS DR9. The data we use includes two files, the LAMOST MRS General Catalog, `dr9_v1.0_MRS_catalogue.fits.gz`, and the LAMOST MRS Parameter Catalog `dr9_v1.0_MRS_stellar.fits.gz`, which are downloaded from http://www.lamost.org/dr9/v1.0/catalogue . The LAMOST comparison samples have three groups: **A**. In section 5.1, the obsevations that fail to meet the following quality criteria are removed: (i) `rv_b_flag` equal to 0, (ii) absolute value of `rv_b0_err` $<$ 8, `snr_b` $>$ 10 and (iii) valid `rv_b0`. The final comparison sample contains 25,253 observations including 6,916 in the Pilot Survey and 18,337 in the Formal Survey. **B**. In section 5.2, for each LAMOST star with multiple observations from the sample **A**, the occurrence with the highest `snr_b` is kept. The final comparison sample contains 8,583 stars. **C**. In Section 5.3, the stars from the sample **B** are further filtered after dropping out those without valid `logg_lasp`, `teff_lasp` and `feh_lasp`. The final comparison sample contains 8,429 stars.

RAVE DR6. The data we use includes five tables from https://www.rave-survey.org , which are dr6_sparv, dr6_classification, dr6_madera, dr6_gauguin_madera and dr6_obsdata. For each RAVE star observed multiple times, the occurrence with the highest `snr_med_sparv` is kept. In addition, the stars that meet the following quality criteria remain: (i) `flag_1_class` set to `a`, `d`, `g`, `h`, `n`, `o`, `t` and `u`, (ii) absolute value of `correction_rv_sparv` $<$ 10, `correlation_coeff_sparv` $>$ 10, `hrv_error_sparv` $<$ 8, `snr_med_sparv` $\geq$ 10 and (iii) valid `hrv_sparv`, `logg_cal_madera`, `teff_cal_madera` and `m_h_cal_madera`. The final RAVE DR6 comparison sample contains 1504 stars.

GALAH DR3. The data we use sources from the `GALAH_DR3_main_allstar_v2.fits` file and the `GALAH_DR3_VAC_rv_v2.fits` file, which can be downloaded from https://www.galah-survey.org/dr3/the_catalogues/ . The stars that fail to meet the following quality criteria are removed: (i) `use_rv_flag`, `flag_sp` and `flag_fe_h` all three equal to 0, (ii) `snr_c3_iraf` $\geq$ 10 and (iii) valid `rv_nogr_obst`, `logg`, `teff` and `fe_h`. The final GALAH DR3 comparison sample contains 1450 stars.

Additionally, Figure 14 provides the distribution of atmospheric parameters for the above four survey catalogs, which supports the investigation of atmospheric parameter trends in Section 5.3.

REFERENCES

Boulkaboul, A., Damerdji, Y., Morel, T., et al. 2022, MNRAS, 517, 1849, doi: 10.1093/mnras/stac2674

Brandt, G. M., Brandt, T. D., & McCully, C. 2020, AJ, 160, 25, doi: 10.3847/1538-3881/ab929c

Buder, S., Sharma, S., Kos, J., et al. 2021, MNRAS, 506, 150, doi: 10.1093/mnras/stab1242

Chen, J., Luo, A. L., Li, Y.-B., et al. 2022, ApJ, 931, 133, doi: 10.3847/1538-4357/ac66de

Chubak, C., Marcy, G., Fischer, D. A., et al. 2012, arXiv e-prints, arXiv:1207.6212. https://arxiv.org/abs/1207.6212

Cropper, M., Katz, D., Sartoretti, P., et al. 2018, A&A, 616, A5, doi: 10.1051/0004-6361/201832763

De Silva, G. M., Freeman, K. C., Bland-Hawthorn, J., et al. 2015, MNRAS, 449, 2604, doi: 10.1093/mnras/stv327

Deng, L.-C., Newberg, H. J., Liu, C., et al. 2012, Research in Astronomy and Astrophysics, 12, 735, doi: 10.1088/1674-4527/12/7/003

Huang, Y., Liu, X. W., Chen, B. Q., et al. 2018, AJ, 156, 90, doi: 10.3847/1538-3881/aacda5

Huber, D., Chaplin, W. J., Chontos, A., et al. 2019, AJ, 157, 245, doi: 10.3847/1538-3881/ab1488

Katz, D., Sartoretti, P., Guerrier, A., et al. 2022, arXiv e-prints, arXiv:2206.05902, doi: 10.48550/arXiv.2206.05902

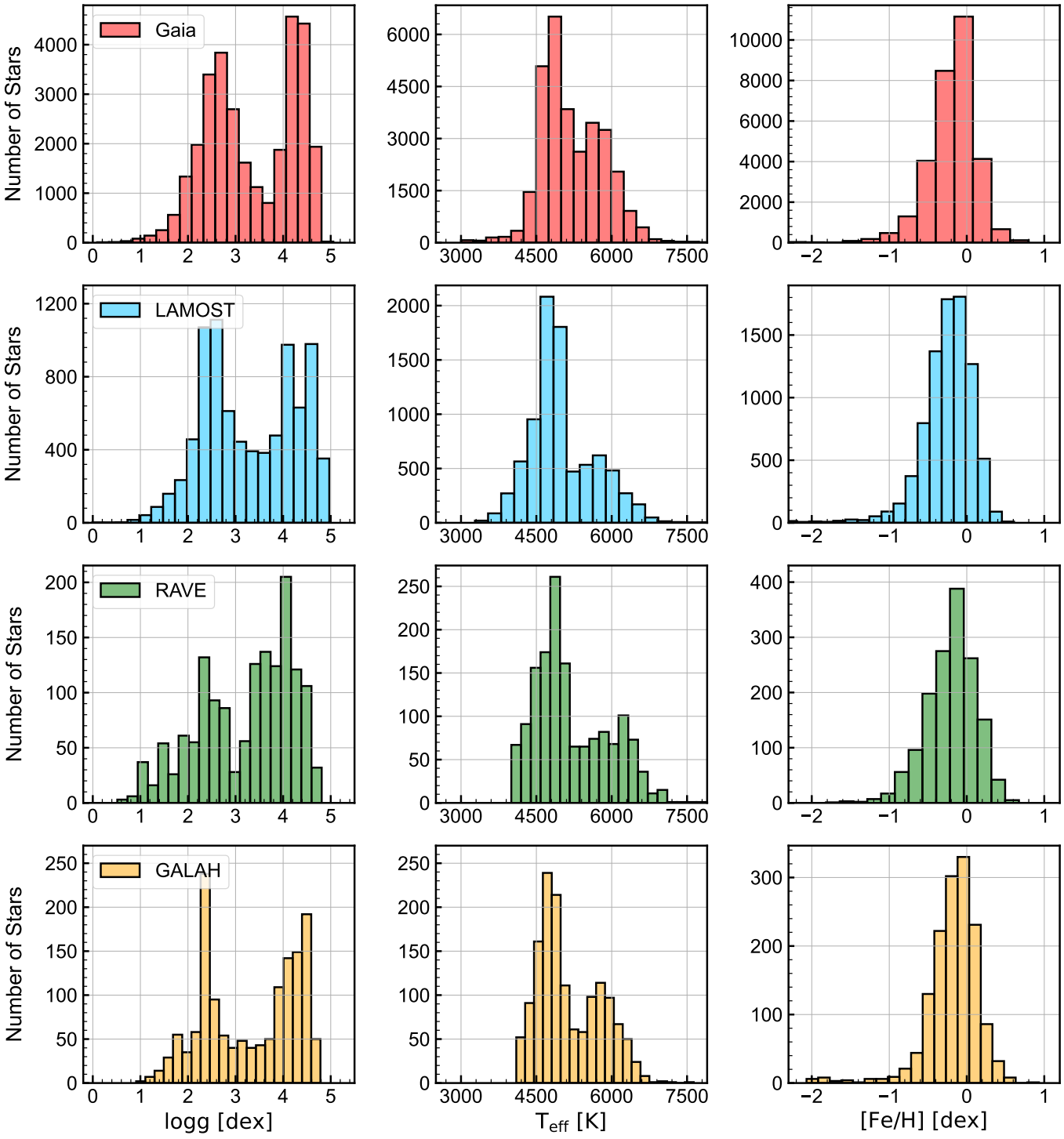

Figure 14. Histograms of the atmospheric parameters, i.e., surface gravity (logg), effective temperature (T_{eff}) and metallicity ([Fe/H]), from left to right. Arranged from top to bottom are Gaia, LAMOST, RAVE and GALAH, respectively.

Kounkel, M., Covey, K. R., Stassun, K. G., et al. 2021, AJ, 162, 184, doi: 10.3847/1538-3881/ac1798

Li, C.-H., Benedick, A. J., Fendel, P., et al. 2008, Nature, 452, 610, doi: 10.1038/nature06854

Lindegren, L., & Dravins, D. 2003, A&A, 401, 1185, doi: 10.1051/0004-6361:20030181

Liu, C., Fu, J., Shi, J., et al. 2020, arXiv e-prints, arXiv:2005.07210, doi: 10.48550/arXiv.2005.07210

Luhn, J. K., Wright, J. T., Howard, A. W., & Isaacson, H. 2020, AJ, 159, 235, doi: 10.3847/1538-3881/ab855a

Luo, A. L., Zhao, Y.-H., Zhao, G., et al. 2015, Research in Astronomy and Astrophysics, 15, 1095, doi: 10.1088/1674-4527/15/8/002

Newton, E. R., Irwin, J., Charbonneau, D., et al. 2016, ApJ, 821, 93, doi: 10.3847/0004-637X/821/2/93

Nidever, D. 2021, dnidever/doppler: Cannon and Payne models, v1.1.0, Zenodo, Zenodo, doi: 10.5281/zenodo.4906681

Nidever, D. L., Marcy, G. W., Butler, R. P., Fischer, D. A., & Vogt, S. S. 2002, ApJS, 141, 503, doi: 10.1086/340570

Nidever, D. L., Holtzman, J. A., Allende Prieto, C., et al. 2015, AJ, 150, 173, doi: 10.1088/0004-6256/150/6/173

Rosenthal, L. J., Fulton, B. J., Hirsch, L. A., et al. 2021, ApJS, 255, 8, doi: 10.3847/1538-4365/abe23c

Sartoretti, P., Katz, D., Cropper, M., et al. 2018, A&A, 616, A6, doi: 10.1051/0004-6361/201832836

Soubiran, C., Jasniewicz, G., Chemin, L., et al. 2013, A&A, 552, A64, doi: 10.1051/0004-6361/201220927

—. 2018, A&A, 616, A7, doi: 10.1051/0004-6361/201832795

Steinmetz, M., Zwitter, T., Siebert, A., et al. 2006, AJ, 132, 1645, doi: 10.1086/506564

Steinmetz, M., Matijevič, G., Enke, H., et al. 2020, AJ, 160, 82, doi: 10.3847/1538-3881/ab9ab9

Tsantaki, M., Pancino, E., Marrese, P., et al. 2022, A&A, 659, A95, doi: 10.1051/0004-6361/202141702

Udry, S., Mayor, M., & Queloz, D. 1999a, in Astronomical Society of the Pacific Conference Series, Vol. 185, IAU Colloq. 170: Precise Stellar Radial Velocities, ed. J. B. Hearnshaw & C. D. Scarfe, 367

Udry, S., & Santos, N. C. 2007, ARA&A, 45, 397, doi: 10.1146/annurev.astro.45.051806.110529

Udry, S., Mayor, M., Maurice, E., et al. 1999b, in Astronomical Society of the Pacific Conference Series, Vol. 185, IAU Colloq. 170: Precise Stellar Radial Velocities, ed. J. B. Hearnshaw & C. D. Scarfe, 383

Wang, R., Luo, A. L., Chen, J. J., et al. 2019, ApJS, 244, 27, doi: 10.3847/1538-4365/ab3cc0

Xiang, M., & Rix, H.-W. 2022, Nature, 603, 599, doi: 10.1038/s41586-022-04496-5

Yanny, B., Rockosi, C., Newberg, H. J., et al. 2009, AJ, 137, 4377, doi: 10.1088/0004-6256/137/5/4377

Zasowski, G., Cohen, R. E., Chojnowski, S. D., et al. 2017, AJ, 154, 198, doi: 10.3847/1538-3881/aa8df9

Zhang, B., Li, J., Yang, F., et al. 2021, ApJS, 256, 14, doi: 10.3847/1538-4365/ac0834

Zhao, Y., & Dumusque, X. 2021, in Plato Mission Conference 2021. Presentations and posters of the online PLATO Mission Conference 2021, 33, doi: 10.5281/zenodo.5553367